Journal of Sound and Vibration 333 (2014) 2241–2252

Contents lists available at ScienceDirect

Journal of Sound and Vibration

journal homepage: www.elsevier.com/locate/jsvi

A bifurcation-based coupled linear-bistable system for microscale mass sensing

R.L. Harne *, K.W. Wang

Department of Mechanical Engineering, University of Michigan, Ann Arbor, MI 48109-2125, USA

ARTICLE INFO

Article history:
Received 19 May 2013
Received in revised form
15 December 2013
Accepted 17 December 2013
Handling Editor: L.N. Virgin
Available online 15 January 2014

ABSTRACT

Bifurcation-based mass sensing provides for dramatically enhanced detection sensitivity and less performance deterioration due to measurement noise as compared to frequency shift-based methods. Recent bifurcation-based mass sensing studies have employed directly excited nonlinear oscillators to induce critical jump events, but the approaches may still require active tracking hardware to determine exact mass adsorption, could induce adverse nonlinear phenomena by prolonged excitation near the bifurcation, and are limited in the number and versatility of jump events. In this work, an alternative sensor architecture and method for mass sensing are presented to address these concerns. The architecture is based upon the coupling of a host linear structure to a small bistable inclusion. It is shown that the sensor enables unique functionality including means for passive mass quantification and direct adjustment of bifurcation sweeping rate for reliable detection and enhanced robustness to noise. Deterministic, stochastic, and non-stationary analyses demonstrate the operational principles and sensitivities of the method while experiments with proof-of-concept samples corroborate analytical results and give clear evidence of the advantages of the new approach.

1. Introduction

Micro/nanoelectromechanical systems (M/NEMS) have proliferated as low-cost and high-performance sensors across a broad range of applications, including magnetic field detection, gyroscopic orientation, and biological, chemical, and atomic mass monitoring [1,2]. The latter field has received dramatic research attention due to analytical and experimental demonstration that these systems may probe to quantum scales, indicating that mass/force detection ability of micro- and nanomechanical sensors is useful for day-to-day applications (e.g. mercury detection [3]) as well as for fundamental physics exploration [4–6].

A common protocol for microscale mass sensing is a derived translation between mass adsorbed upon the resonating sensor and a detectable change in the fundamental mode natural frequency [1–6]. Although this is a useful approach, researchers continue to tackle with the inherently nonlinear dynamics of resonators on these scales which makes an expression between accumulated mass and natural frequency shift less straightforward than ideally obtained with linearity [1]. While some have investigated methods to offset one nonlinearity by another (e.g. introducing softening Duffing effects to counteract hardening Duffing behaviors [7,8]), recent research has developed alternative sensing approaches based upon the inherent nonlinear dynamics of MEMS. These latter studies harness nonlinear bifurcation phenomena which serve as dramatic

* Corresponding author.
E-mail address: rharne@umich.edu (R.L. Harne).

0022-460X/$ - see front matter © 2013 Elsevier Ltd. All rights reserved.
http://dx.doi.org/10.1016/j.jsv.2013.12.017

amplitude-based sensing measures, following a methodology earlier developed for the Josephson junction or bifurcation amplifier [9].

One significant benefit of bifurcation-based sensing is that the metric of change is an unmistakable jump or drop in sensor response amplitude once the bifurcation is crossed. The techniques are much less susceptible to damping than frequency shift-based approaches because bifurcations may be activated regardless of damping so long as the excitation level exceeds a critical threshold. While frequency shift-based sensing sensitivity is highly influenced by various noise forms and limited by hardware resolution capability, bifurcation-based sensing sensitivity and resolution is theoretically constrained only by thermomechanical noise and Brownian motion [9–11], which is an enticing potential for the mass/force sensing field. For MEMS, bifurcations associated with parametric resonance [12–15], dynamic pull-in [16], and the saddle-node of a softening Duffing oscillator [17] have demonstrated significant mass sensing sensitivity enhancement. Additional benefits include substantially less deterioration of detection performance due to measurement noise than frequency shift-based approaches [12,18,19] and some bifurcation-based approaches offer reduced implementation complexity by eliminating phase-tracking hardware [16,17].

There have been two primary protocols demonstrated for bifurcation-based microscale mass sensing. Both employ the foundational idea that mass accumulation affects bifurcation conditions. In the first, an excitation frequency sweep towards a bifurcation frequency is conducted and the frequency which triggers the jump event is determined; repeating the process yields a time-variation of the shift due to added mass. A bifurcation analysis of Mathieu′s equation for the parametric resonator provides an expression of jumping frequency as a function of system parameters: thus, specific change in the frequency denotes a quantity of adsorbed mass [13]. While the success of this approach is less susceptible to measurement noise and damping than frequency shift-based sensing methods [12,14,18], the technique is still vulnerable to early or delayed jump events [20,21] and requires a collection of active control and tracking hardware. The second protocol is a passive technique that employs a constant frequency excitation just below the bifurcation, allowing for mass adsorption to reduce the critical frequency and induce the jump [16,17]; thus, the second approach detects a threshold. Because mass adsorption may be very slow, the challenges to reliably utilize this technique are tied to the intrinsic phenomena associated with prolonged excitation near bifurcation, including noise-induced transitions [20] and period-doubling cascades [22–24]. Finally, while additional bifurcations due to super- and subharmonics have been demonstrated [16], no bifurcation-based mass sensing works have yet explored means by which to sequentially employ such phenomena to determine the mass adsorbed in the time span between consecutive jumps, thereby achieving mass quantification without excess control and tracking hardware. Therefore, of the remaining challenges in the area of bifurcation-based mass sensing, some key issues are: utilizing bifurcations to passively quantify mass adsorption over time without need for active hardware; avoiding prolonged excitation near the bifurcation frequency which may induce strongly nonlinear phenomena and inhibit reliable detection; and a degree of sensor adaptability to changing testing conditions which may help optimize sweeping through bifurcations for reliable jump event activation and hence mass detection.

To address these concerns, this work presents an alternative bifurcation-based sensing protocol and sensor architecture which conceptually combines frequency shift- and bifurcation-based detection techniques. In the following sections, the operational principle and system architecture are described. Analytical treatment of the system is conducted and validated by experiments to demonstrate the detection strategy and sensor versatility and to initially evaluate noise sensitivities. Further experimental examples verify the successful utilization of the approach and a summary discussion is provided to review the advancements offered by the new bifurcation-based mass sensing system.

2. Architecture and operational principle detail

2.1. Bistable sensor component and capabilities

In contrast to the past bifurcation-based sensor architectures, the sensor in this study utilizes a statically and dynamically bistable element. Bistable MEMS enable broad functionality and as a result have been the focus a wide body of recent research. Numerous studies have explored their application as switches [25,26], valves or actuators [27,28], and non-volatile memory [29,30]. The nonlinearities of bistable MEMS have been probed in detail regarding electrostatic actuation dependence [31,32], imperfections and deviations from ideal fabrication [33–35], and snap through activation [36,37].

A key advantage of bistable elements for bifurcation-based mass sensing is exemplified by evaluating a characteristic steady-state response amplitude to excitation level profile, two examples of which are shown in Fig. 1 as computed from the derivations of the authors′ earlier investigation [38]. For given normalized excitation frequency ω, the level of harmonic excitation h may lead to either small amplitude (intrawell or single-well) or highly energetic (interwell or cross-well) responses. With the bistable element initially oscillating around a stable equilibrium, for example point A in Fig. 1(a), gradually increased excitation level will lead to triggering a bifurcation that induces the energetic interwell response, the B to C jump which represents a significant increase in steady-state response amplitude. Once the bistable element is captured in the interwell response, reduction of excitation level follows a hysteretic trajectory such that the energetic response is sustained down to the critical point E. At this point, further decrease in excitation level activates the E to F bifurcation downwards in amplitude. When excited at a different steady-state excitation frequency, Fig. 1(b), several hysteretic trajectories are observed because three unique dynamics may be induced: a low amplitude intrawell, a higher amplitude intrawell, and energetic interwell responses.

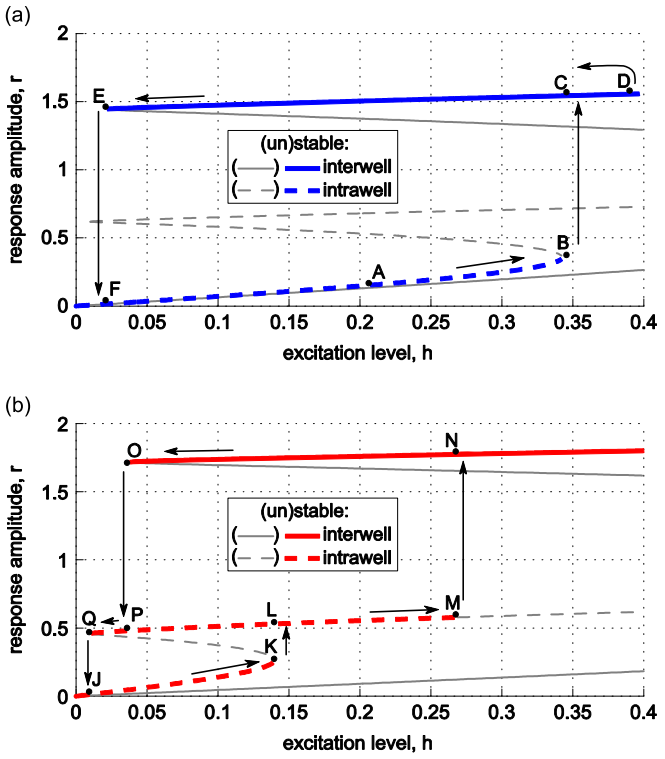

Fig. 1. Bistable element displacement response amplitude r dependency upon excitation level h, computed from Ref. [38] with $\gamma=0.02$ and $\beta=1$.

In the prior study [38], the authors derived closed form expressions for the critical set of system parameters leading to these jumps. In a mass sensing context, the critical parameter set may be expressed in terms of changing sensor mass. While a single bifurcation is sufficient for threshold detection, to extend the practical utility of the sensor by quantifying mass adsorption over time at least two jumps must be activated and the difference computed between the two critical masses. The externally-controlled bifurcation-based sensing approaches, using parametric resonators, meet this necessity by repeatedly activating the same bifurcation using excitation frequency sweeps into the progressively decreasing critical jumping frequency [12–14]. This methodology will in fact be used in Section 4 as one demonstration of the proof-of-concept test sample for the proposed sensing methodology. Yet the inherent availability of at least two jumps, as observed in Fig. 1(a), indicates that mass quantification may be achieved *passively* using a constant frequency of excitation, so long as the influence of adsorbed mass leads to an increasing and then decreasing change in excitation level. Unfortunately, direct mass accumulation upon a bistable oscillator does not play a role in changing its excitation conditions. As a result, the sensor architecture developed in this research is designed in such a way that mass adsorption leads to an effective change in excitation *level* for the bistable element despite potentially utilizing constant excitation conditions.

2.2. Two degrees-of-freedom sensor architecture

This requirement will be shown to be satisfied by a two degrees-of-freedom (DOF) sensor architecture. In its most essential form, the sensor may be composed of an excited primary linear structure having a small bistable inclusion attached to its free end (or generalized displacement coordinate). In the proof-of-concept sample as shown in Fig. 2, this architecture is realized via two coupled beams: a small inset beam is located at the primary beam free end and buckled through the repulsive interaction of magnets. To ensure that only the inset beam is deflected by the magnetic interaction, the inset is machined with reduced thickness, approximately 480 μm as compared to host beam thickness 1180 μm. This fabrication detail is evident in Fig. 2 (c,d) which also demonstrate the two post-buckled stable states of the small inset beam. The proof-of-concept sample includes a recessed track that allows tailoring of the bistability by modifying the repulsive magnet gap which is related to the axial buckling load. As shown in Fig. 2(b,e), the host beam is cantilevered from an excitation source; in this way, the primary structure is a cantilevered beam while the inset bistable beam is cantilevered from the end of the host beam opposite to the excitation. For consistency, throughout the remainder of this work, term “sensor” will denote the complete coupled linear-bistable system. Additionally, the linear member of the proof-of-concept system will be referred to as the host beam, whereas remarks about any potential coupled linear-bistable system will refer to this element as the host structure, since the underlying resonator need not be a beam.

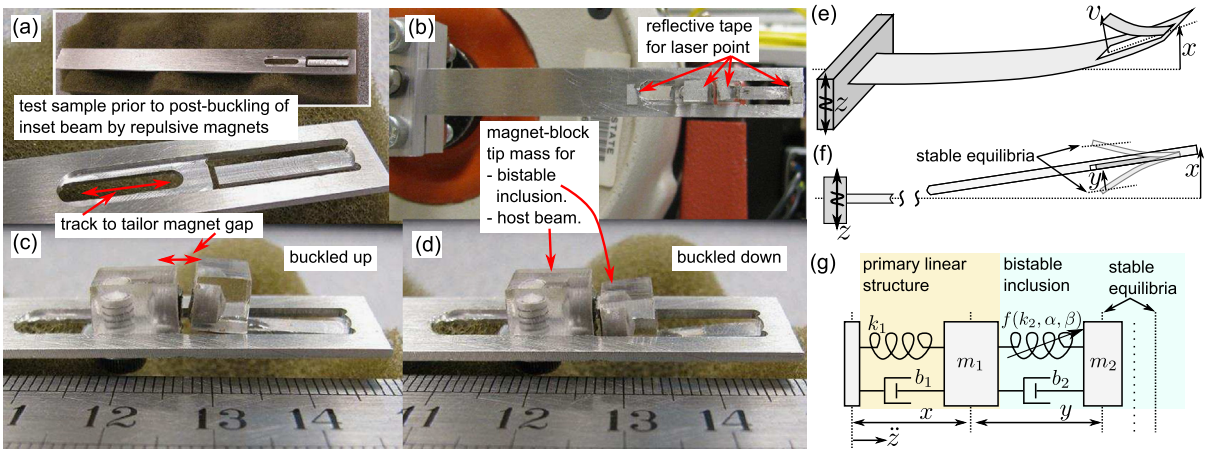

Fig. 2. Proof-of-concept photograph details. (a) Host beam with inset beam, showing fabrication details prior to magnet attachment. (b) System cantilevered from shaker for testing. (c) and (d) Buckled states of inset bistable beam due to magnetic repulsion. Schematic of modeling coordinates (e) before and (f) after coordinate transformation for bistable beam inclusion. (g) Lumped parameter equivalent model.

2.3. Sensor operational strategy

Although the sensor may be employed using controlled excitation sweeps that repeatedly activate the bifurcation to quantify mass accumulation over time, as will be demonstrated in Section 4, the sensor architecture also empowers a unique mass sensing strategy that integrates the advantages of frequency shift-based and bifurcation-based methods. If the bistable inclusion constitutes a small amount of the total sensor mass and has a linear natural frequency sufficiently greater than the host structure, then the two DOF sensor steady-state response around the fundamental mode is effectively identical to a single DOF system response. Therefore, the linear dynamics of the sensor around its fundamental mode are equivalently expressed by the response-to-excitation transfer function magnitude of a driven, damped harmonic oscillator [39]:

$$H = 1/\sqrt{(1-\omega^2)^2+(2\zeta\omega)^2} \tag{1}$$

where the normalized excitation frequency $\omega = \Omega/\Omega_1$ is the ratio of the excitation to the natural frequencies, and damping ratio is $\zeta = b/2\sqrt{km}$. From the perspective of the small bistable inclusion, the influence of the host structure around the fundamental mode is that of a *variable gain excitation source*, such that the excitation level h in Fig. 1 is related to amplitude H, with maximum gain when the excitation frequency aligns with the fundamental mode, $\omega = 1$. In the vibration energy harvesting research community, this design concept has been described as a "dynamic magnifier" for small energy harvester systems attached to larger resonant sub-structures [40,41].

For the sensor architecture, these influences are utilized to passively induce an excitation level sweep for the bistable inclusion so as to activate two bifurcations in sequence for mass quantification. In this way, the normalized excitation frequency ω changes because the fundamental natural frequency is reduced due to adsorbed mass, despite excitation conditions remaining constant. An illustration of this utility is provided in Fig. 3 to assist in the following description of the passive sweeping strategy. Fig. 3 illustrates the progressive reduction in frequency of a fundamental mode response, H, due to increased modal mass (thus as both Ω_1 and ζ decrease proportional to $m^{-1/2}$). For a comparable sensor, this would represent adsorbed mass on the host structure since the host is presumed to represent the bulk of the net sensor mass. Fig. 3 also highlights representative points from Fig. 1(a) with respect to a constant excitation frequency, Ω.

Thus, the two DOF sensor architecture may be excited at constant frequency Ω initially less than the fundamental natural frequency Ω_1 prior to mass accumulation, such that the normalized excitation frequency $\omega < 1$, and at constant excitation level such that the bistable inclusion is initially in low amplitude intrawell oscillations, like point A in Fig. 1(a) which is depicted by point A* in Fig. 3. Therefore, the influence of mass adsorption upon the much larger host structure reduces the fundamental mode frequency. Eventually, a critical excitation level working upon the bistable inclusion is reached which induces the first bifurcation, like the B–C jump in Fig. 1(a) and shown as B*–C* in Fig. 3. Continued mass adsorption reduces the fundamental mode frequency until it coincides with the fixed excitation frequency, $\omega = 1$, point D*, and represents the maximum excitation level gain passed to the bistable inclusion. Further mass adsorption indicates the sensor is excited above the fundamental mode resonance, $\omega > 1$, and thus the gain passed to the bistable inclusion reduces, at some point finally leading to the subsequent bifurcation like E–F in Fig. 1(a) and shown as E*–F* in Fig. 3. In summary, the design of the sensor is such that it may be utilized to *passively* induce an excitation *level* sweep for the bistable inclusion because excitation conditions remain constant: mass adsorption alone leads to variation in sensor responses. These factors are more obviously grasped by specific example and, to this end, an analytical model of the sensor architecture is developed.

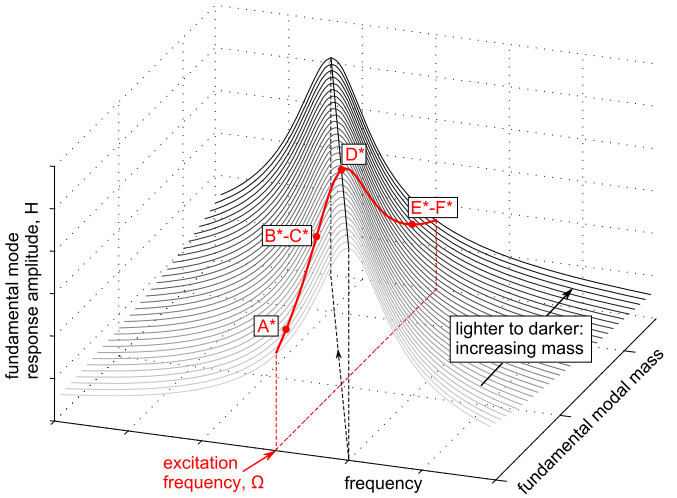

Fig. 3. Fundamental mode response amplitude shifting in frequency due to increased modal mass. Letter labels illustrate representative points from Fig. 1(a) in the context of activating sequential bifurcation for the two DOF sensor architecture using constant excitation conditions.

3. System modeling and operational demonstration

3.1. Governing equations

The governing equations are derived according to lumped parameter assumptions which are appropriate for many continuously-distributed microscale systems [1,2,8]. Due to the specific test setup, the system is modeled as undergoing base excitation, although a similar equation system may be formulated for direct forcing of the host structure (e.g. a piezoceramic actuator on the clamped host beam end). The equations are initially derived using the host structure displacement relative to base motion, x, and the relative displacement between the bistable element and host structure, v, as the response coordinates. The initial coordinate convention with respect to the sensor architecture sub-systems is depicted in Fig. 2(e). Application of Newton's 2nd law then yields

$$m_1(\ddot{x}+\ddot{z})+b_1\dot{x}+k_1x-b_2\dot{v}-\Lambda'(v)=0 \tag{2a}$$

$$m_2(\ddot{v}+\ddot{x}+\ddot{z})+b_2\dot{v}+\Lambda'(v)=0 \tag{2b}$$

Here, m_i, b_i, k_i are effective mass, damping, and linear stiffnesses of the sub-systems, respectively; $\Lambda(v)$ is an expression of the potential energy of the bistable element as a function of the relative displacement coordinate v; and operators $(\cdot)$ and $()'$ denote time and spatial derivatives, respectively. In this study, the classical, symmetric quartic potential energy profile (the double-well) is utilized which is one possible representation of the potential energy of a beam buckled by repulsive magnet interactions [42].

$$\Lambda(v)=-\frac{1}{2}k_{2L}v^2+\frac{1}{4}k_{2NL}v^4 \tag{3}$$

The spatial derivative of the potential energy, $\Lambda'=\partial\Lambda/\partial v$, is the restoring force from which may be computed the fixed points of the bistable sub-system: $\Lambda'(v)=0\rightarrow v^*=\pm\sqrt{k_{2L}/k_{2NL}}$. Here, v^* are the stable equilibria which are symmetric with respect to a central unstable configuration. Next, a coordinate transformation is applied by defining $y=v-v^*$ such that the bistable inclusion response coordinate y is zero at one of the stable positions. Substitution of this transformation into equation system (2) and a series of simplifications leads to equation system (4):

$$m_1\ddot{x}+b_1\dot{x}+k_1x-b_2\dot{y}-k_2y[1+\alpha y+\beta y^2]=-m_1\ddot{z} \tag{4a}$$

$$m_2\ddot{y}+(1+\mu)[b_2\dot{y}+k_2y(1+\alpha y+\beta y^2)]-\mu(b_1\dot{x}+k_1x)=0 \tag{4b}$$

Here, $k_2=2k_{2L}$, while $\alpha=3\sqrt{k_{2NL}/k_{2L}}$ and $\beta=k_{2NL}/k_{2L}$ are stiffness proportionality constants; $\mu=m_2/m_1$ is the ratio of bistable to host structure effective masses; and $-\ddot{z}=Z_a\sin\Omega t$ is the harmonic base acceleration of amplitude Z_a and frequency Ω. To compensate for asymmetries evident between the bistable inclusion stable equilibria, the proportionality constants α and β may be modifed to deviate from the prior expressions; the additional equilibria are then positioned at $v^*=[-\alpha\pm\sqrt{\alpha^2-4\beta}]/2\beta$. Note that equation system (4) includes linear, quadratic, and cubic terms for the bistable inclusion displacement y due to the coordinate transformation. For clarity, the generalized coordinates respecting the coupled linear-bistable beam system are illustrated in Fig. 2(f) while the lumped parameter modeling conventions are shown in Fig. 2(g).

3.2. Numerical demonstration of system operation

The system parameter set of the fabricated test samples are first experimentally identified and presented in Table 1. The bistable inclusion is seen to possess asymmetry between the stable equilibria around the unstable position and this is reflected in the identified proportionality constants α and β. The fundamental mode natural frequency of the system is $\Omega_1/2\pi=61.3$ Hz while the second mode occurs at $\Omega_2/2\pi=184$ Hz. Next, the parameter set is scaled down to microscale platform dimensions, taking into account design factors of microscale bistable structures regarding asymmetries induced via residual stress [29,30,43,44]. The scaled parameter set is provided in Table 2. In the numerical demonstration, to represent mass adsorption on the sensor over time, the mass of the host structure is a time-dependent quantity such that its mass increases at a mass ratio rate of $+0.001$ per second, reflective of a target analyte entering and diffusing in an environment during a MEMS mass sensing application. Mass ratio is defined as the accumulated mass over the baseline host structure mass m_1 and the rate was arbitrarily selected for this demonstration. In the following simulation, the host structure is excited at a constant frequency that is 99.4 percent of the fundamental mode natural frequency prior to mass accumulation, $\Omega=0.994\Omega_1$. Finally, to demonstrate the passive mass quantification strategy of the proposed sensor architecture, equation system (4) is numerically integrated with a fourth-order Runge–Kutta routine using parameters given in Table 2, and the results are plotted in Fig. 4.

At the beginning of simulation, because the system is excited at a frequency slightly less than the fundamental mode, such that $\omega=\Omega/\Omega_1<1$, and the bistable element is excited within a linear response regime, both elements of the sensor have almost identical response amplitudes, apparent in Fig. 4 by the coincident results. During this time, the bistable inclusion is confined to intrawell response, similar to point A in Fig. 1(a). Gradually, however, mass accumulates upon the host structure such that the reduced fundamental mode natural frequency draws closer to the excitation frequency, $\omega\rightarrow1$, magnifying the transmitted excitation level to the bistable inclusion and ultimately activating the bistable element bifurcation from intrawell to interwell responses, like the B–C jump in Fig. 1(a). Now the bistable inclusion exhibits large displacement and velocity amplitudes and the host structure response is substantially perturbed. Following continued mass accumulation such that the fundamental mode natural frequency is reduced to the extent that the constant excitation frequency is above resonance, $\omega>1$, the ability of the bistable inclusion to sustain interwell response is compromised and an E–F type of bifurcation downwards in response is observed. The mass quantity adsorbed from jump up to jump down may be determined from one of two ways. With knowledge of the time elapsed between sequential bifurcations and the rate of mass adsorption, one may directly compute the mass accumulation. This method is not as useful in practice because the rate of accumulation is likely unknown. The alternative approach is to conduct a bifurcation analysis for equation system (4) to derive closed-form expressions relating bifurcations to the host structure mass. This is comparable to the prior study [38] from which Fig. 1 was plotted, although in the present case the system is a two DOF architecture and the analysis will yield more complex expressions. Derivation of such expressions are one part of on-going efforts.

From the example in Fig. 4, the signaling that bifurcations are crossed is uniquely determined depending on how a sensing signal is extracted from the system. The individual plots of Fig. 4 depict the variety of measurements that would be available based on how transduction is configured to monitor either the host structure or bistable inclusion. Thus, in a configuration that monitors a response related to velocity, the sensed bifurcation event is denoted by sudden amplitude modulation in host structure response or dramatic increase in the bistable inclusion response, Fig. 4(b), both of which are accompanied by a transient spike in additional harmonic content (spectra not shown here). Monitoring displacement of the bistable inclusion provides the most notable indication of change due to the biased mean displacement during the period of interwell vibrations, Fig. 4(a). The latter unambiguous indicator is not obtained in previous bifurcation-based MEMS mass sensing studies that have explored monostable oscillator systems.

Table 1
System parameters identified from test setup.

m_1 (g)	m_2 (g)	b_1 (N s/m)	b_2 (N s/m)	Z_a (m/s^2)
3.52	0.705	0.0673	0.0228	15
k_1 (N/m)	k_2 (N/m)	α (1/m)	β (1/m^2)	
637	766	1.27×10^3	3.20×10^5	

Table 2
System parameters used in simulation for sequential jump events.

m_1 (ng)	m_2 (ng)	b_1 (nN s/m)	b_2 (nN s/m)	Z_a (m/s^2)
5	0.1	471	18.2	7.0
k_1 (N/m)	k_2 (N/m)	α (1/m)	β (1/m^2)	
7.11	0.299	4.57×10^5	4.64×10^{10}	

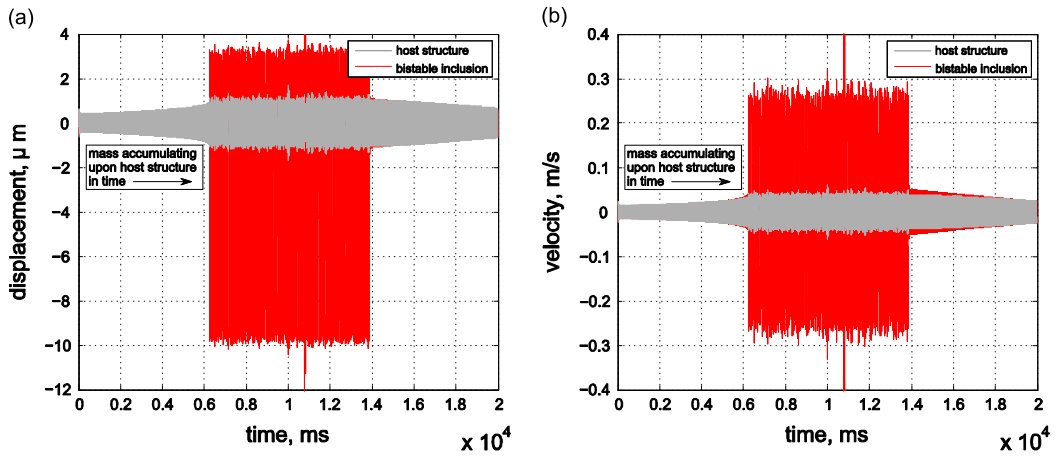

Fig. 4. Demonstration of sequential bifurcation activation due to mass accumulation upon host structure. (a) Response displacements and (b) velocities.

4. Experimental investigation

Since this work presents proof-of-concept results of a new sensing method and architecture, the aim of the following experimental study is more focused on demonstrating some of the mass sensing enhancements described earlier and less focused on highlighting improved detection accuracy. The simulated results in Fig. 4 exemplified the *passive* sensing strategy that may quantify adsorbed mass. This strategy was recently experimentally demonstrated by the authors in a comparable study of a coupled linear-bistable system composed of a host beam and attached bistable circuitry [45] and gives credence to the methods strong potential. Therefore, to explore the alternative sensing protocol for the proposed sensor, in the following example, bifurcation triggering via the controlled frequency sweep approach is investigated. However, the results will concurrently provide important insight regarding the passive detection strategy.

The test setup is shown in Fig. 2(b); the laser point for velocity measurement is directed to the mass of the host beam end, composed of the magnet-block assembly on the recessed track. Before each experiment, wax mass is measured using a microgram scale and incrementally applied to the host beam free end. Low-level white noise base excitation is used to determine the fundamental mode natural frequency from the frequency response function (frf) of beam velocity to base acceleration. Then, for a constant excitation level, the excitation frequency is slowly swept from 55 Hz at a rate of $+0.05$ Hz/s into the critical jumping point. The trial is stopped once the jump event is activated to avoid excessive fatiguing of the thin bistable inset beams during extended periods of interwell response. The critical bifurcation frequency is determined; as described earlier, the change of the critical frequency may be used to compute the accumulated mass quantity following suitable bifurcation analysis. The process is then repeated following further incremental addition of wax mass.

Fig. 5(a) presents the time series of an example experimental frequency sweep test in which case no added wax is applied. As the excitation frequency gradually sweeps toward the fundamental mode of the system, the vibration of the host beam becomes magnified, so as to greatly amplify the net excitation upon the small bistable inclusion. Simulated results, Fig. 5(b,c), using equation system (4) and the experimental system parameters of Table 1 are in very good agreement with the measurements, Fig. 5(a). Partially along the frequency sweep at which point the instantaneous frequency is approximately 59 Hz, an order-3 harmonic is induced within the asymmetric bistable inclusion which is observed via the host beam as a small spike in velocity prior to leveling out again in response. The experimental observation of this feature is closely replicated in numerical simulation, Fig. 5(b). It must be emphasized that this phenomena is not inherent in the use of the linear-bistable system design (attested by the absence of comparable phenomena in Fig. 4) but was conclusively determined to be a coincidence of the exact parameters of the fabricated samples (and therefore parameters used in simulation). As indicated in Section 3, the second mode linear natural frequency of the system is 184 Hz, which is coincidentally almost exactly three times the fundamental 61.3 Hz. It is known that for a nonlinear two DOF system having a 1:3 ratio of natural frequencies, excitation close to the fundamental will induce a strong higher harmonic response which may suddenly become manifest [46]. This is an undesirable coincidence of the fabricated samples (primarily due to the exact degree of magnetic repulsion-buckling employed which partially governs this frequency) and fractional or integer multiples of the natural frequencies should be avoided in future sample fabrication. Considering again characteristics of the frequency sweep in Fig. 5, the bistable inclusion response is pushed continually closer to the bifurcation point by the steady amplification of the host beam response as harmonic excitation sweeps closer to the fundamental mode natural frequency. In the experiment, the bifurcation is activated and observed by a surge and spike in host beam velocity, Fig. 5(a). In simulation, the bifurcation is likewise accompanied by a spike in beam velocity, Fig. 5(b), while the bistable inclusion jumps to the other potential well, Fig. 5(c). The overall good agreement between the measured and simulated results helps to validate the modeling assumptions and formulation, and verifies that system parameters are correctly identified which is necessary to support the continued investigations of this work.

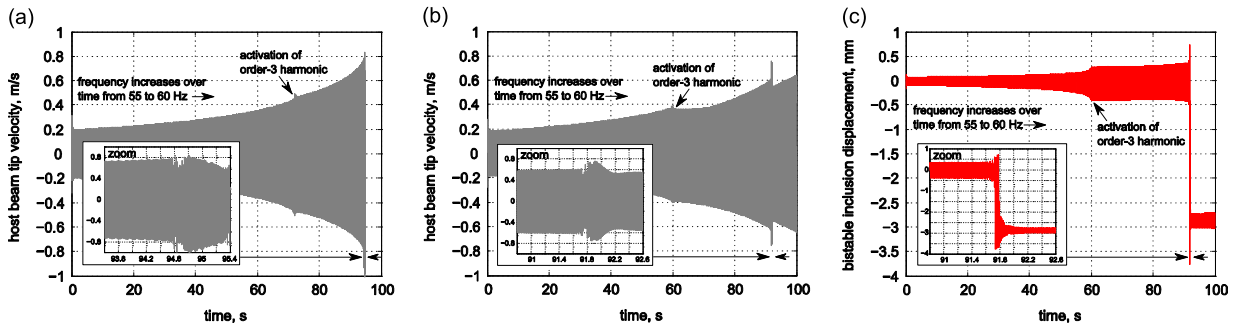

Fig. 5. Frequency sweep into bifurcation. (a) Experiment: host beam velocity. (b) Simulation: host beam velocity. (c) Simulation: bistable inclusion displacement. Inset images denote zoomed views of bifurcation activation.

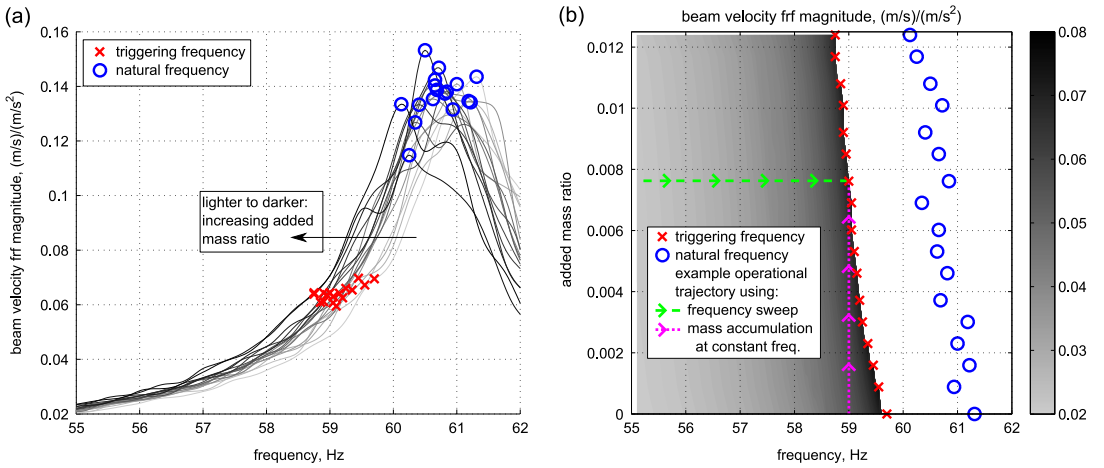

Fig. 6. (a) Host beam frf due to low-level white noise input denoting natural frequencies and the corresponding triggering frequencies for cases of mass addition. (b) Measured frf magnitudes for all cases of added mass ratio and triggering frequencies.

Having observed a typical experimental response trajectory, the results of experimental frequency sweeps for a range of added mass up to 0.012 mass ratio are collected in Fig. 6. Fig. 6(a) demonstrates how the measured frfs of the host beam are affected as mass accumulates upon the free beam end. The peaks of the frfs, identified as the fundamental mode natural frequencies, are plotted as circles and influences of noise, damping, and finite time duration for sampling inhibit desirable sharp resonant peaks, thus making traditional frequency shift-based mass sensing a less reliable indicator of accumulating mass.

Fig. 6(b) plots frf results for the trials conducted for each case of mass addition. The contour represents the instantaneous frf amplitudes measured during frequency sweeps; the transition from grayscale contour to the unshaded region denotes the initial triggering of interwell oscillations. The bifurcation frequencies are shown as crosses which define the boundary between the intrawell to interwell oscillations, like the B–C jump in Fig. 1(a). While natural frequency is observed to non-uniformly reduce in consequence to mass accumulation, the triggering frequency consistently reduces upon each case of mass addition. Consequently, there is no mistaking mass accumulation using bifurcation-based detection as compared to tracking the fundamental natural frequency (circles).

In Fig. 6(b), the dashed and dotted lines, respectively, depict operational trajectories the sensor would follow using either the controlled sweep method or the passive strategy with constant excitation conditions. When employing the passive strategy, it is shown that the constant excitation frequency is a means by which to tailor the quantity of mass that initially triggers the sensor: frequencies closer to the bifurcation require less added mass to induce the first jump. Although each test was stopped when the bistable inclusion interwell response was initially activated, it should be recalled that for continued sweeps, either by frequency or accumulating mass, the second bifurcation downward in response is eventually encountered. The second bifurcation is not essential for the controlled sweeping approach because repeated activation of the initial bifurcation yields sufficient information (bifurcation frequency shift) from which adsorbed mass may be quantified. However, for the passive sensing strategy, the second bifurcation is required and the close connection between the dotted trajectory in Fig. 6(b) and the analogous example in Fig. 3 should be emphasized.

As illustrated in Fig. 3, the passive mass sensing strategy utilizes a range of excitation level gains passed to the bistable inclusion, which is similar to a *path* of fundamental mode responses at given constant excitation frequency. For the proof-of-concept sample, a portion of this trajectory is shown as the dotted line in Fig. 6(b) up until the initial bifurcation point (cross) which is equivalent to B*–C* in Fig. 3. Envisioning the trends of Fig. 6(b) to continue to higher mass ratios, the

remainder of the trajectory would extend the vertical dotted line "over" the fundamental mode peak (the range denoted by circles) and "down" the opposite side to reach the next critical frf level, i.e., the equivalent E*–F* level from Fig. 3. The rate of following this path, and therefore the rate of jump activation, has important implications in bifurcation-based sensing, and it is to this matter that the present study turns.

5. Stochastic modeling and noise sensitivities

Bifurcations are inherently stochastic processes since their activation may be inadvertently induced by noise [9,10,20]. Given that mass sensing is necessarily a non-stationary process—that is, mass accumulates at a finite rate over time—the link between stochastic influences in bifurcation-based sensing and the rate of bifurcation activation is pivotal for accurate detection because premature or delayed jump events could reduce detection reliability [20–22,24]. Therefore, for initial insight into the stochastic sensitivities of the proposed bifurcation-based sensing method and two DOF sensor, equation system (4) is expressed in Itô stochastic differential equation (SDE) form for the following investigation. In addition to the harmonic base excitation, a stochastic process $\zeta(t)$ acts upon the host structure:

$$\mathrm{d}x = \begin{bmatrix} x_2 \\ \{-k_1x_1 - b_1x_2 + k_2x_3(1+\alpha x_3+\beta x_3^2) + b_2x_4\}/m_1 + Z_a \sin \omega t \\ x_4 \\ \{\mu(k_1x_1+b_1x_2) - (1+\mu)[k_2x_3(1+\alpha x_3+\beta x_3^2)+b_2x_4]\}/m_2 \end{bmatrix} \mathrm{d}t + \begin{bmatrix} 0 \\ S \\ 0 \\ 0 \end{bmatrix} \mathrm{d}B \tag{5a}$$

$$\mathbf{x} = [x_1, x_2, x_3, x_4]^T = [x, \dot{x}, y, \dot{y}]^T;\ \langle \zeta(t) \rangle = 0;\ \ \langle \zeta(t)\zeta(t_0) \rangle = S^2\delta(t-t_0) \tag{5b}$$

where $-\ddot{z} = Z_a \sin \omega t + \zeta(t)$. The stochastic process $\zeta(t)$ is additive white Gaussian noise of intensity S^2 and zero mean, where $\mathrm{d}B/\mathrm{d}t = \zeta(t)$. In microscale applications, additive white noise processes $\zeta(t)$ commonly represent uncertainties including thermomechanical fluctuations, Brownian motion, and self-heating [4,11,47].

Prior to exploring noise dependencies, equation system (5) is experimentally validated for responses near the fundamental mode. Fig. 7(a,c) present measured and simulated beam velocity to base acceleration frf curves, respectively, of the system in Fig. 2(b) when excited by low-level white noise ($S = 0.1$) as mass is incrementally added to the host beam free end. For each case of added mass ratio, a 15 s time series of system response to white noise is measured or simulated. For the numerical simulations, base acceleration is not included ($Z_a = 0$) and equation system (5) is integrated using the SDE toolbox in MATLAB. The frf results are normalized to the peak of the case without added mass. As mass is added to the end of the cantilevered host beam, the resonance frequencies—peaks of the plots Fig. 7(a,c)—non-uniformly shift downwards in frequency, Fig. 7(b). Collectively, noise interferences, damping, and the finite duration of the time series make the resonances less sharply defined than ideal. Good agreement is seen comparing experimental and simulated trends, and Fig. 7(b) shows that residual norms of the shifting natural frequency exhibit a similar deviation against linear fits. These findings verify that stochastic and damping influences are appropriately modeled with respect to system parameters in Table 1, and support the further use of the model to evaluate sensitivities of the proposed system architecture and sensing method as functions of noise level and the bifurcation activation rate.

The responses of equation system (5) having additive noise and periodic base excitations are then simulated using the sweeping styles earlier explored: constant excitation level with (a) controlled frequency sweeps or (b) constant excitation frequency and progressive mass accumulation over time. The important parameter distributions to consider are the values of the measure (frequency or mass accumulation) that occur at the jump event. In this work, excitation-to-noise ratio (ENR) is used to denote the dominance of the harmonic base excitation relative to additive stochastic effects. For example, the

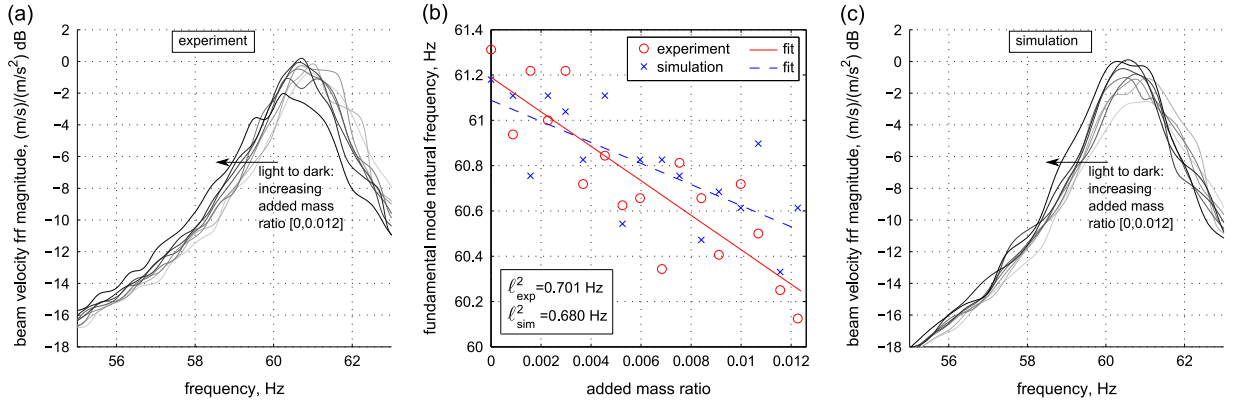

Fig. 7. (a) Experimentally measured frf around the fundamental mode as added mass increases (light to dark). (b) Measured and numerically simulated fundamental mode natural frequencies as mass increases, with linear fits and residual norms (in inset). (c) Comparable simulated frf responses due to stochastic excitation.

root-mean-square value of an 0 dB ENR additive stochastic process is equal to the periodic base acceleration amplitude. Thus, a simulation with 0 dB ENR is effectively noise-dominated while a 40 dB ENR simulation is primarily influenced by the harmonic base excitation. In microscale mass sensing applications, ENR may be tailored to overcome noise by applying higher drive levels at the cost of inducing greater nonlinearities in response [1].

Fig. 8 presents the results of the investigations for the two sweeping styles as functions of ENR level and various sweeping rates. The bar heights represent mean values of the monitored parameter—frequency of first crossing in (a) and added mass at first crossing in (b)—determined from 40 trials, while the error bars are one standard deviation from the mean. It should be noted that simulations conducted with slower sweep rate and high ENR (low additive noise) induce the most *accurate* triggering values because such cases approach the limiting condition of stationary and deterministic bifurcation activation [20].

Fig. 8(a) plots results of the frequency sweep studies. In these simulations, a frequency sweep begins at 55 Hz, and several forward sweep rates are employed from 0.005 to 0.2 Hz/s. It is seen that for high ENR the individual cases of frequency sweep rate converge to distinct values of the first crossing parameter, here the frequency of the bifurcation event, and that faster sweeps exhibit greater deviation and mean values of bifurcation frequency. This indicates that faster sweeps induce *delayed* bifurcations, that is, jump events which occur for critical values in excess of the stationary and deterministic result; as judged by Fig. 8(a) from the slowest sweep rate at high ENR, the latter is approximately 59.63 Hz. In contrast, for low ENR (high noise), *premature* bifurcations are activated for all sweeping rates. This may seem counterintuitive but reflects the fact that noise may activate a bifurcation in advance of the system reaching the deterministic critical condition [20]. Some of these findings are similar to those experimentally observed in recent bifurcation-based mass sensing investigations using variable-rate frequency sweeping strategies [21]. Our additional insight for the present system is provided by the deliberate inclusion of noise since stochastic influences are difficult to eliminate in microscale mass sensing contexts.

Fig. 8(b) shows results for the mass accumulation sweeps where base acceleration is held at constant frequency of 59 Hz while mass gradually accumulates on the host beam end. Several added mass ratio (m.r.) rates are utilized. Similar to the frequency sweeping method, low noise (high ENR) and slow mass accumulation rates converge to specific m.r. values to trigger (approximately 0.0048) and exhibit narrow standard deviations around this mean; again, this value represents the approximate stationary and deterministic critical m.r. value to activate the bifurcation. As the ENR is gradually reduced and noise becomes more influential, the additive noise frequently induces premature jumps, notably influencing the results from approximately around 15–20 dB ENR, and the accumulated mass necessary to cross the bifurcation is reduced (premature bifurcation). By comparing the range of critical activation parameters between Fig. 8(a,b), it may be concluded that bifurcation activation is substantially more sensitive to change in mass accumulation rate than the frequency sweeping rate. For example at 15 dB ENR, both Fig. 8(a,b) plot a range of sweeping rates spanning a factor of 20 (0.005–0.1 Hz/s, and 0.0001–0.002 m.r./s) but the change in mean critical jumping frequency is only about 0.5 percent whereas the mean critical absorbed mass changes by almost 100 percent. These observations are not intended to be a comprehensive evaluation of the sensing method's overall sensitivities, but represent first efforts to examine the noise dependencies exhibited by the two forms of bifurcation sweeping for the proposed sensor platform.

In light of the prior findings, a final important point may be made. To take advantage of the unique passive mass sensing strategy, it is clear that due to the high variation exhibited in Fig. 8(b), an optimized rate of mass accumulation is required in a given noise environment for accurate bifurcation activation, and hence mass quantification. The proposed two DOF sensor architecture provides novel means by which to govern this rate, regardless of mass accumulation rate. As described in Section 2.3, the two DOF sensor induces an effective excitation level sweep upon the bistable inclusion which is related to the amplitude of the fundamental mode response for a constant excitation frequency. It was experimentally shown in

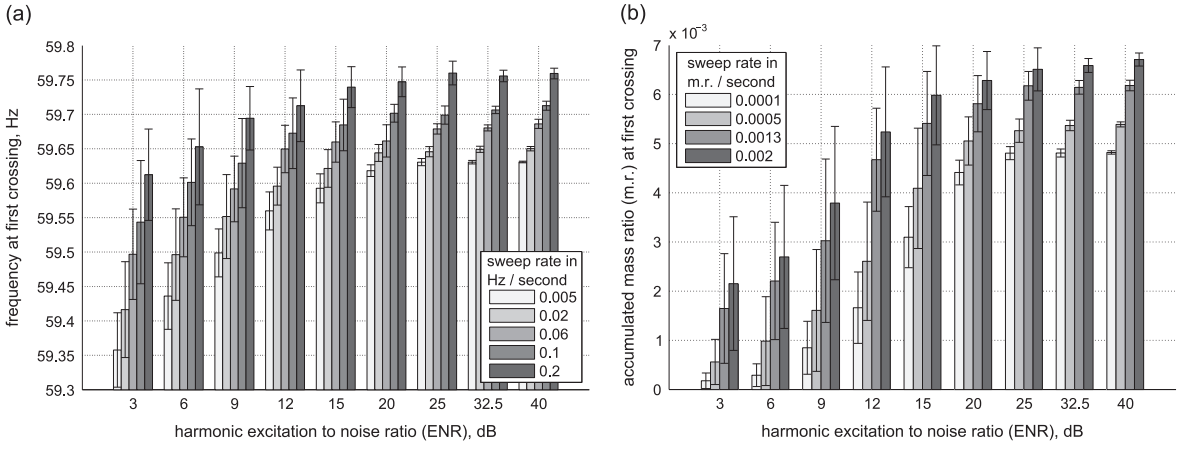

Fig. 8. Dependence on additive noise excitation contribution for (a) excitation frequency sweeps into the bifurcation and (b) mass accumulation sweeps into the bifurcation (m.r.=mass ratio).

Section 4 by the dotted line trajectory in Fig. 6(b), that adjustment of this frequency determines the mass accumulation required to trigger the initial bifurcation. In a similar manner, the *rate* of the effective excitation level sweep for the bistable inclusion is related to the rate of growth of the fundamental mode response which, using the one DOF analogy of Section 2.3, is given by

$$\mathrm{d}H/\mathrm{d}\omega = 2\omega[(1-\omega^2)-2\zeta^2]/[(1-\omega^2)^2+(2\zeta\omega)^2]^{3/2} \tag{6}$$

Like the adjustment of the initial gain level passed to the bistable inclusion, the sweep rate is directly adjusted by way of the constant excitation frequency and overall sensor base excitation level. As seen in Fig. 8, the sweep rate controls the probability distribution of parameter values which trigger the jump event and therefore the viability of the detection strategy. This is a important tool for maintaining repeatable and accurate mass quantification and increases sensor robustness to inevitable microscale noise processes. Further stochastic sensitivity studies of simulated and experimental responses are required to reach deeper conclusions in these regards but it is clear that the proposed sensor and mass sensing methods provide new opportunities for reliable and effective detection using bifurcation-based strategies.

6. Concluding discussion

In this study, an alternative method and architecture for bifurcation-based mass sensing is presented which has specific promise for microscale applications. The architecture empowers a unique strategy for passive mass quantification that would greatly advance the practicality of bifurcation-based microscale mass sensing by eliminating need for external tracking hardware. The coupled linear-bistable sensor enables a high degree of adjustability for consistent and accurate bifurcation activation and hence mass detection. Numerically simulated results of modeled sensor responses are in good agreement with experimental data and provide strong initial evidence of the new potentials afforded by the coupled linear-bistable architecture. Continued investigations are required to thoroughly examine the stochastic and sweeping sensitivities of the sensor and detection strategies, and to develop closed-form bifurcation criteria which are needed to passively quantify mass by the activation of two bifurcations in sequence. These are on-going efforts which will be further supported by additional proof-of-concept experimental studies as well as investigations with microscale sensor fabrications.

Acknowledgments

This research was supported in part by the University of Michigan Collegiate Professorship fund. The authors wish to thank Mr. Zhen Wu for fabricating experimental samples used in this study.

References

[1] R. Lifshitz, M.C. Cross, Nonlinear dynamics of nanomechanical and micromechanical resonators, H.G. Schuster (Ed.), *Reviews of Nonlinear Dynamics and Complexity*, Volume 1, Wiley, Weinheim2008, pp. 1–52.
[2] M.I. Younis, *MEMS Linear and Nonlinear Statics and Dynamics*, Springer, New York, 2011.
[3] T. Thundat, E.A. Wachter, S.L. Sharp, R.J. Warmack, Detection of mercury vapor using resonating microcantilevers, *Applied Physics Letters* 66 (1995) 1695–1697.
[4] K.L. Ekinci, Y.T. Yang, M.L. Roukes, Ultimate limits to inertial mass sensing based upon nanoelectromechanical systems, *Journal of Applied Physics* 95 (2004) 2682–2689.
[5] M. Li, H.X. Tang, M.L. Roukes, Ultra-sensitive NEMS-based cantilevers for sensing, scanned probe and very high-frequency applications, *Nature Nanotechnology* 2 (2007) 114–120.
[6] J. Chaste, A. Eichler, J. Moser, G. Ceballos, R. Rurali, A. Bachtold, A nanomechanical mass sensor with yoctogram resolution, *Nature Nanotechnology* 7 (2012) 301–304.
[7] M.I. Younis, A.H. Nayfeh, A study of the nonlinear response of a resonant microbeam with an electric actuation, *Nonlinear Dynamics* 31 (2003) 91–117.
[8] M. Sato, B.E. Hubbard, A.J. Sievers, Colloquium: Nonlinear energy localization and its manipulation in micromechanical oscillator arrays, *Reviews of Modern Physics* 78 (2006) 137–157.
[9] R. Vijay, M.H. Devoret, I. Siddiqi, Invited review article: The Josephson bifurcation amplifier, *Review of Scientific Instruments* 80 (2009) 111101.
[10] A.B. Zorin, Quantum-limited electrometer based on single cooper pair tunneling, *Physical Review Letters* 76 (1996) 4408–4411.
[11] J.R. Vig, Y. Kim, Noise in microelectromechanical system resonators, *IEEE Transactions on Ultrasonics, Ferroelectrics, and Frequency Control* 46 (1999) 1558–1565.
[12] W. Zhang, K.L. Turner, Noise analysis in parametric resonance based mass sensing, *Proceedings of IMECE* 2004 *ASME International Mechanical Engineering Congress and Exposition*, Anaheim, California, 2004, pp. IMECE2004-61412.
[13] W. Zhang, K.L. Turner, A mass sensor based on parametric resonance, *Proceedings of Solid-State Sensor, Actuator and Microsystems Workshop*, Hilton Head Island, South Carolina, 2004, pp. 49–52.
[14] W. Zhang, K.L. Turner, Application of parametric resonance amplification in a single-crystal silicon micro-oscillator based mass sensor, *Sensors and Actuators A* 122 (2005) 23–30.
[15] J.F. Rhoads, S.W. Shaw, K.L. Turner, The nonlinear response of resonant microbeam systems with purely-parametric electrostatic actuation, *Journal of Micromechanics and Microengineering* 16 (2006) 890–899.
[16] M.I. Younis, F. Alsaleem, Exploration of new concepts for mass detection in electrostatically-actuated structures based on nonlinear phenomena, *Journal of Computational and Nonlinear Dynamics* 4 (2009) 021010.
[17] V. Kumar, J.W. Boley, Y. Yang, H. Ekowaluyo, J.K. Miller, G.T.-C. Chiu, J.F. Rhoads, Bifurcation-based mass sensing using piezoelectrically-actuated microcantilevers, *Applied Physics Letters* 98 (2011) 153510.
[18] Z. Yie, M.A. Zielke, C.B. Burgner, K.L. Turner, Comparison of parametric and linear mass detection in the presence of detection noise, *Journal of Micromechanics and Microengineering* 21 (2011) 025027.
[19] C.B. Burgner, L.A. Shaw, and K.L. Turner, A new method for resonant sensing based on noise in nonlinear MEMS, *Proceedings of the* 2012 *IEEE* 25*th International Conference on Micro Electro Mechanical Systems* (MEMS), Paris, 2012, pp. 511–514.

[20] N. Berglund, B. Gentz, *Noise-Induced Phenomena in Slow-Fast Dynamical Systems: A Sample-Paths Approach*, Springer, London, 2000.
[21] C.B. Burgner, K.L. Turner, N.J. Miller, S.W. Shaw, Parameter sweep strategies for sensing using bifurcations in MEMS, Solid-State Sensors, Actuators, and Microsystems Workshop, Hilton Head Island, South Carolina, 2010, pp. 130–133.
[22] C. Baesens, Slow sweep through a period-doubling cascade: delayed bifurcations and renormalisation, *Physica D* 53 (1991) 319–375.
[23] A.H. Nayfeh, M.I. Younis, E.M. Abdel-Rahman, Dynamic pull-in phenomenon in MEMS resonators, *Nonlinear Dynamics* 48 (2007) 153–163.
[24] C.-H. Lu, R.M. Evan-Iwanowski, Period doubling bifurcation problems in the softening Duffing oscillator with nonstationary excitation, *Nonlinear Dynamics* 5 (1994) 401–420.
[25] J.S. Go, Y.H. Cho, B.M. Kwak, K. Park, Snapping microswitches with adjustable acceleration threshold, *Sensors and Actuators A* 54 (1996) 579–583.
[26] M.T.A. Saif, On a tunable bistable MEMS – theory and experiment, *Journal of Microelectromechanical Systems* 9 (2000) 157–170.
[27] B. Wagner, H.J. Quenzer, S. Hoerschelmann, T. Lisec, M. Juerss, Bistable microvalve with pneumatically coupled membranes, *Proceedings of MEMS* 1996, 1996, pp. 384–388.
[28] J. Qiu, J.H. Lang, A.H. Slocum, A curved-beam bistable mechanism, *Journal of Microelectromechanical Systems* 13 (2004) 137–146.
[29] D. Roodenburg, J.W. Spronck, H.S.J. van der Zant, W.J. Venstra, Buckling beam micromechanical memory with on-chip readout, *Applied Physics Letters* 94 (2009) 183501.
[30] M. Bagheri, M. Poot, L. Mo, P.H.P. Wolfram, H.X. Tang, Dynamic manipulation of nanomechanical resonators in the high-amplitude regime and non-volatile mechanical memory operation, *Nature Nanotechnology* 6 (2011) 726–732.
[31] S. Krylov, B.R. Ilic, S. Lulinsky, Bistability of curved microbeams actuated by fringing electrostatic fields, *Nonlinear Dynamics* 66 (2011) 403–426.
[32] M.I. Younis, H.M. Ouakad, F.M. Alsaleem, R. Miles, W. Cui, Nonlinear dynamics of MEMS arches under harmonic electrostatic actuation, *Journal of Microelectromechanical Systems* 19 (2010) 647–656.
[33] L. Ruzziconi, S. Lenci, M.I. Younis, An imperfect microbeam under an axial load and electric excitation: nonlinear phenomena and dynamical integrity, *International Journal of Bifurcation and Chaos* 23 (2013) 1350026.
[34] L. Ruzziconi, A.M. Bataineh, M.I. Younis, W. Cui, S. Lenci, Nonlinear dynamics of an electrically actuated imperfect microbeam resonator: Experimental investigation and reduced-order modeling, *Journal of Micromechanics and Microengineering* 23 (2013) 075012.
[35] S.A. Alkharabsheh, M.I. Younis, Dynamics of MEMS arches of flexible supports, *Journal of Microelectromechanical Systems* 22 (2013) 216–224.
[36] K. Das, R.C. Batra, Pull-in and snap-through instabilities in transient deformations of microelectromechanical systems, *Journal of Micromechanics and Microengineering* 19 (2009) 035008.
[37] K. Das, R.C. Batra, Symmetry breaking, snap-through and pull-in instabilities under dynamic loading of microelectromechanical shallow arches, *Smart Materials and Structures* 18 (2009) 115008.
[38] R.L. Harne, M. Thota, K.W. Wang, Concise and high-fidelity predictive criteria for maximizing performance and robustness of bistable energy harvesters, *Applied Physics Letters* 102 (2013) 053903.
[39] D.J. Inman, *Engineering Vibration*, 2nd ed. Prentice Hall, Upper Saddle River, New Jersey, 2001.
[40] O. Aldraihem, A. Baz, Energy harvester with a dynamic magnifier, *Journal of Intelligent Material Systems and Structures* 22 (2011) 521–530.
[41] W. Zhou, G.R. Penamalli, L. Zuo, An efficient vibration energy harvester with a multi-mode dynamic magnifier, *Smart Materials and Structures* 21 (2012) 015014.
[42] B. Andò, S. Baglio, C. Trigona, N. Dumas, L. Latorre, P. Nouet, Nonlinear mechanism in MEMS devices for energy harvesting applications, *Journal of Micromechanics and Microengineering* 20 (2010) 125020.
[43] D.R. Southworth, L.M. Bellan, Y. Linzon, H.G. Craighead, J.M. Parpia, Stress-based vapor sensing using resonant microbridges, *Applied Physics Letters* 96 (2010) 163503.
[44] D.J. Joe, Y. Linzon, V.P. Adiga, R.A. Barton, M. Kim, B. Ilic, S. Krylov, J.M. Parpia, H.G. Craighead, Stress-based resonant volatile gas microsensor operated near the critically buckled state, *Journal of Applied Physics* 111 (2012) 104517.
[45] R.L. Harne, K.W. Wang, Robust sensing methodology for detecting change with bistable circuitry dynamics tailoring, *Applied Physics Letters* 102 (2013) 203506.
[46] P.R. Sethna, Steady-state undamped vibrations of a class of nonlinear discrete systems, *Journal of Applied Mechanics* 27 (1960) 187–195.
[47] A.N. Cleland, Thermomechanical noise limits on parametric sensing with nanomechanical resonators, *New Journal of Physics* 7 (2005) 235.